Journal of Catalysis 260 (2008) 305–314

Contents lists available at ScienceDirect

Journal of Catalysis

www.elsevier.com/locate/jcat

Kinetic modeling of the oxidation of CO on Fe_2O_3 catalyst in excess of O_2

Steffen Wagloehner, Dirk Reichert, Daniel Leon-Sorzano, Peter Balle, Bastian Geiger, Sven Kureti *

Institut für Technische Chemie und Polymerchemie, Universität Karlsruhe, D-76128 Karlsruhe, Germany

ARTICLE INFO

Article history:
Received 9 May 2008
Revised 29 August 2008
Accepted 23 September 2008
Available online 31 October 2008

Keywords:
Catalytic oxidation
CO
Fe_2O_3
Mechanism
DRIFTS
Isotopic labeling
Kinetics
Numeric modeling
Mean field approximation
Thermodynamic consistency

ABSTRACT

This work addresses the oxidation of CO under oxygen-rich conditions using a Fe_2O_3 model catalyst. Based on in situ DRIFTS studies, isotopic labeling, and kinetic examinations performed in a gradient-free loop reactor an Eley–Rideal type mechanism is postulated. This mechanism includes the dissociative adsorption of O_2 on active Fe sites, followed by reaction of surface oxygen with gaseous CO, producing CO_2. Furthermore, a mean field model is constructed for numeric modeling and simulation of the CO oxidation, as well as calculation of the Fe_2O_3 surface coverage. The kinetic model represents a network of six elementary reactions using Arrhenius-based rate expressions. The comparison between measured and calculated data shows that the model describes the experiments well. Kinetic parameters for the elementary reactions are obtained from the literature or by fitting calculations. To reduce the number of free parameters, the patterns of O_2 TPD and CO_2 TPD are modeled numerically. To validate the model, the kinetic parameters are used to simulate catalytic data, which agree fairly well with the corresponding experimental results. The reaction of surface oxygen species with gas-phase CO is considered to be the rate-determining step in CO oxidation on an Fe_2O_3 catalyst. In addition, the thermodynamic consistency of the kinetic parameters is proven.

1. Introduction

Diesel engines exhibit the highest efficiency for automotive applications. As a consequence, their low fuel consumption leads to a reduced production of the greenhouse gas CO_2. However, a serious constraint of diesel engines is the emission of air pollutants, including hydrocarbons (HC), carbon monoxide (CO), nitrogen oxides (NO_x), and soot [1]. Several after-treatment techniques for removing these pollutants from the oxygen-rich diesel exhaust have been developed [2,3]. The use of diesel particulate filters (DPFs) to decrease soot emissions has been studied. In such systems, the soot is mechanically separated from the exhaust stream. The accumulation of the soot necessitates a regeneration process, however. This regeneration can be performed discontinuously by increasing temperature through the postinjection of fuel combined with oxidation of the resulting unburned hydrocarbons and CO on a Pt precatalyst [4]. In addition, the ignition temperature of the soot can be lowered by the introduction of a cerium- or iron-containing fuel additive [4] or by a catalyst coated onto the DPF substrate, such as Pt or CeO_2 [5]. The continuous regeneration of DPF systems is provided by the continuously regenerating trap (CRT) technique, in which soot conversion is initiated by the strong oxidant NO_2 [6,7]. The required NO_2 is produced by oxidation of NO on a Pt precatalyst.

The use of selective catalytic reduction (SCR) and NO_x storage reduction (NSR) catalysts for the removal of NO_x from diesel exhaust has been studied. The NSR procedure is based on the periodic adsorption and reduction of NO_x [8–10]; the catalysts consist of precious metals, primarily Pt, as well as basic adsorbents, such as Al_2O_3 and $BaCO_3$. The platinum component supports the oxidation of NO into NO_2, which is subsequently stored by the adsorbents. When the storage capacity is reached, rich exhaust conditions are established momentarily by engine management systems, in which NO_x desorbs from the substrate and is reduced by H_2, CO, and hydrocarbons on the precious metals. A disadvantage of the NSR technique is the susceptibility of the basic adsorbents to sulfur poisoning [11]. In the SCR technique, NO_x is continuously reduced by NH_3 on TiO_2-supported WO_3/V_2O_5 catalysts, resulting in the selective formation of nitrogen [12,13]. The ammonia required for SCR can be produced on board by hydrolysis of nonhazardous urea, which is stored in another tank. But a disadvantage of the SCR procedure is the toxic nature of the V_2O_5 component; thus, harmless catalytic systems with promising SCR performance (e.g., the zeolite Fe-ZSM5) have been developed [14,15].

In contrast to soot and NO_x the pollutants HC and CO can be simply converted in the oxygen-rich diesel exhaust by using Pt or Pd oxidation catalysts [2]. The mechanism and kinetics of the catalytic oxidation of HC and CO on Pt have been investigated in depth by several groups [16–18]. Furthermore, numerous studies on nanosized Au catalysts useful for CO oxidation have been published [19], which demonstrate that these materials have in-

* Corresponding author. Fax: +49 721 608 2816.
E-mail address: kureti@ict.uni-karlsruhe.de (S. Kureti).

0021-9517/$ – see front matter
doi:10.1016/j.jcat.2008.09.018

sufficient thermal stability for practical applications. In addition, some iron-containing oxides also have been reported to be effective in CO oxidation, either as a catalyst (e.g., $LaFeO_3$ [20], $LaFe_{1-x}(Cu,Pd)_xO_3$ [21], $Fe_2O_3/Cr_2O_3/Al_2O_3$ [22], Fe_2O_3/SiO_2 [23]) or as a support (e.g., Au/Fe_2O_3 [24], Pd/Fe_3O_4 [25]). Little detail is available on the CO oxidation on Fe_2O_3 based catalysts, however. Consequently, the aim of the present work was to study the mechanism and kinetics of the oxidation of CO in an excess of O_2 using a α-Fe_2O_3 catalyst; α-Fe_2O_3 was used as the model sample to exclude interactions of the active sites with a specific support. Based on the mechanistic and kinetic examinations, a kinetic mean field model was constructed to provide insight into the reactions occurring on the surface of Fe_2O_3. The mechanistic examinations were carried out using both isotopic labeling and in situ diffuse-reflectance infrared Fourier transform spectroscopy (DRIFTS). The kinetic studies were performed with a gradient-free loop reactor, and temperature-programmed desorption of O_2 (O_2 TPD) and CO_2 (CO_2 TPD) was conducted to obtain independent kinetic parameters. Finally, for model validation, some simulations were carried out and thermodynamic consistency was proven as well.

2. Experimental

2.1. Catalyst preparation and characterisation

The Fe_2O_3 catalyst was synthesized by the polyvinyl alcohol method as described previously [26], with final calcination in air at 600 °C for 5 h. The catalyst was characterized by powder X-ray diffraction (PXRD), N_2 physisorption, and temperature-programmed reduction by H_2 (HTPR). The PXRD analysis was performed at room temperature on a Siemens D 501 with a Ni-filtered CuK_α radiation source and a rotating sample holder. N_2 physisorption was conducted with a Porotec Sorptomatic 1990. The sample was pretreated at 350 °C for 2 h in vacuum (10^{-4} mbar) and cooled to −196 °C, after which the N_2 isotherm was recorded. The BET surface area (S_{BET}) was derived from the adsorption data recorded at p/p_0 ratios of 0.05–0.30.

In HTPR, 29 mg of catalyst powder (according to 20 mg of Fe) was charged into the quartz glass tube reactor (6 mm i.d.) and fixed with quartz wool. Then the reaction mixture (5 vol% H_2, 95 vol% N_2) was added at a flow of 100 ml/min (STP), and the temperature was increased linearly to 900 °C at a rate of 20 K/min. The temperature was monitored by a K-type thermocouple located directly in front of the sample. The concentration of H_2 was measured continuously with a Shimadzu thermoconductivity detector. For the specific detection of H_2, the water formed was removed by passing the reactor effluents through a cold trap (−50 °C).

2.2. TPD studies

For CO_2 TPD and O_2 TPD, the catalyst was in granular form, to avoid discharge. The sample was pressed into pellets at a pressure of 40 MPa, granulated, and sieved to a size of 125–250 μm. Before TPD, the catalyst was pretreated in an N_2 flow at 500 °C for 30 min, to eliminate possible impurities and obtain reproducible conditions. Then it was cooled to 200 °C, at which point CO_2 or O_2 exposure was initiated. After saturation, the catalyst was flushed with N_2, and the temperature was increased linearly at a rate (β) of 10 K/min. In TPD studies, the total gas flow was maintained at 500 ml/min (STP) while the temperature was monitored by a K-type thermocouple installed directly in front of the sample.

CO_2 TPD was performed with 1.60 g of Fe_2O_3 in a quartz glass tube (11 mm i.d.), whereas exposure to CO_2 was done using a gas mixture of 2 vol% CO_2 and 98 vol% N_2 (Air Liquide). CO_2 was monitored by nondispersive infrared spectroscopy (NDIR) using a Fischer–Rosemount BINOS 5 spectroscope.

O_2 TPD was carried out with a catalyst mass of 15 g in a quartz glass tube (22 mm i.d.). In O_2 exposure, a blend of 2 vol% O_2 and 98 vol% N_2 (Air Liquide) was obtained. O_2 was analysed by chemical ionisation mass spectrometry (CIMS) using a V&F Airsense 500 spectrometer.

2.3. Kinetic studies

For kinetic studies, a commercial cordierite honeycomb (400 cpsi, $d = 10$ mm, $l = 30$ mm) was coated with the Fe_2O_3 catalyst. The substrate was dipped into a slurry of 1 g of grinded Fe_2O_3 ($d < 32$ μm) and 20 ml of water, then heated to 450 °C for 3 h in air. This procedure was repeated several times until a loading of 220 g/l was obtained, corresponding to 500 mg Fe_2O_3.

The kinetic studies were performed using a gradient-free loop reactor with an external gas cycle. The Fe_2O_3-coated honeycomb is packed into an 11-mm-i.d. quartz glass tube, fixed with quartz wool, and pretreated at 500 °C in O_2 flow for 15 min and then for another 15 min in N_2. Then the temperature in the N_2 flow was decreased to 230 °C, at which point the feed was added. The reaction mixture was a blend of the pure components (Air Liquide) dosed from independent flow controllers (MKS Instruments). The feed consisted of 400–7000 ppm CO, 6.0–99.3 vol% O_2, and balance N_2. The total volume flow was 400 ml/min (STP), with a recycling ratio, ψ ($\psi = F_{loop}/F_{out}$), of 110. The temperature was monitored by two K-type thermocouples located directly in front of and behind the honeycomb; the maximum difference of the inlet and outlet temperatures was found to be 10 K. CO and CO_2 were monitored by NDIR (Binos 1.2 for CO and Binos 4b.1 for CO_2, Leybold-Heraeus), and O_2 was detected with a magnetomechanic analyser (Magnos 6G, Hartmann & Braun). The reactor effluents were recorded after steady state was achieved.

In addition, for model validation, CO_2 also was dosed, in varying amounts. These experiments were conducted in an 11-mm-i.d. quartz glass tube reactor, which represented a plug–flow reactor. The total flow was 500 ml/min (STP), and the feed consisted of 7000 ppm CO, 20 vol% O_2, 0–79.3 vol% CO_2, and balance N_2 (Air Liquide).

Mass transfer limitations, which possibly could result from film and pore diffusion, were excluded by estimating the Mears and Weisz criteria [27].

2.4. Isotopic labeling

The isotopic studies were performed with $^{18}O_2$-labeled oxygen (Linde). The quartz glass tube reactor (11 mm i.d.) was charged with Fe_2O_3 granules (320 mg), after which the same pretreatment as described for the kinetic experiments was carried out. After cooling to 260 °C in N_2 flow, the feed, containing 470 ppm $C^{16}O$, 3000 ppm $^{18}O_2$ (Linde), and balance N_2, was added (500 ml/min; STP). The effluent was measured by CIMS.

2.5. DRIFTS studies

The surface species formed in the CO oxidation on Fe_2O_3 catalyst were studied by DRIFTS, using a Nicolet 5700 FTIR spectrometer (Thermo Electron) equipped with an MCT detector and DRIFTS optics (Thermo Mattson). The stainless steel IR cell had a KBr window and was connected to a gas-handling system. The spectra were recorded at 1000–4000 cm^{-1} with an instrument resolution of 2 cm^{-1}. A total of 250 scans per spectrum were accumulated, for a time resolution of 3 min. The temperature of the sample was monitored by a K-type thermocouple placed 2 mm underneath the crucible surface. During the measurements, both the spectrometer and the DRIFTS optics were purged with nitrogen, to avoid air diffusion into the system. Over 24 h, the spectrum of the fresh sample

did not change, and the baseline remained constant. Before the analyses, the Fe_2O_3 powder was charged into the sample holder of the cell and heated for 10 min at 500 °C in N_2 flow (500 ml/min, STP). After cooling to 200 °C or 50 °C, background scans were collected in the N_2 flow. A fresh sample, with its specific background, was used for each DRIFTS experiment. An in situ study of CO oxidation on Fe_2O_3 was performed at 200 °C by passing a mixture of 7000 ppm CO, 6 vol% O_2, and balance N_2 through the cell. Spectra were recorded after reaction times of 10 and 20 min, and then a final spectrum was collected after flushing with N_2. In addition, the catalyst was exposed to a mixture of 7000 ppm CO and 99.3 vol% N_2 at 50 and 200 °C, respectively, for 10 min. The DRIFTS spectra are presented in terms of the Kubelka–Munk transformation, defined as $F(R) = (1-R)^2/(2R)$, with $R = R_s/R_r$, where R_s is the reflectance of the reacted catalyst and R_r is that of the unreacted catalyst.

2.6. Estimation of the sticking coefficient of CO_2

Due to the lack of appropriate literature data, the sticking coefficient of CO_2 on the uncovered Fe_2O_3 catalyst (S^0) was estimated experimentally. The sticking coefficient is important for describing the kinetics of the adsorption of CO_2 on the catalyst and represents a probability factor; it is the ratio of the number of adsorbing species to the number of species exposed to the surface [28]. The experiment was performed similar to CO_2 TPD; that is, after heating at 500 °C and cooling to 200 °C in N_2, the catalyst was exposed to CO_2. The carbon dioxide uptake was determined from the trace of CO_2, whereas the calculation refers to the range of zero to ca. 30% coverage, taking about 38 s. The total amount of CO_2 exposed to the catalyst was calculated based on the time of adsorption, inlet concentration, and flow.

3. Results and discussion

3.1. Catalyst characterisation

The HTPR and PXRD patterns show that the catalyst represents α-Fe_2O_3. The HTPR profile reveals both a low-temperature signal (400 °C) and a high-temperature signal (430–820 °C), whereas the high-temperature to low-temperature peak area ratio was found to be 8, associated with the reduction sequence $Fe_2O_3 \rightarrow Fe_3O_4 \rightarrow Fe$ [29]. In addition, the total conversion of H_2 closely reflected the molar amount of Fe^{3+} used, that is, a ratio of H_2 consumed to Fe consumed of 1.5. All of the reflexes obtained in PXRD can be assigned to α-Fe_2O_3 (ICDD-PDF No. 01-089-0599). The BET surface area was determined to be 15 m^2/g.

The O_2 TPD profile, shown in Fig. 1, exhibits a very weak signal at about 320 °C and a prominent maximum at 745 °C, with a shoulder at 870 °C. The total amount of O_2 desorbed was 0.16 µmol/m^2, denoted as atomic oxygen. Fig. 2 shows the CO_2 TPD pattern, with a single peak at 270 °C. The amount of CO_2 released, 0.68 µmol/m^2, is significantly greater than the amount of oxygen desorbed in O_2 TPD.

3.2. Mechanism and kinetics of catalytic CO oxidation on Fe_2O_3

The effect of O_2 and temperature on the kinetics of the CO oxidation on the Fe_2O_3 catalyst is shown in Fig. 3. The studies were performed with the gradient-free loop reactor at an inlet CO concentration of 7000 ppm, covering a broad range of O_2 content, which provided a substantial database for the kinetic model. As expected, the conversion of CO increased throughout the entire temperature range with increasing O_2 concentration; the effect of O_2 is considered rather weak, however. For instance, at 200 °C, the CO_2 yield was 22% with 6.0 vol% O_2; it was only slightly higher

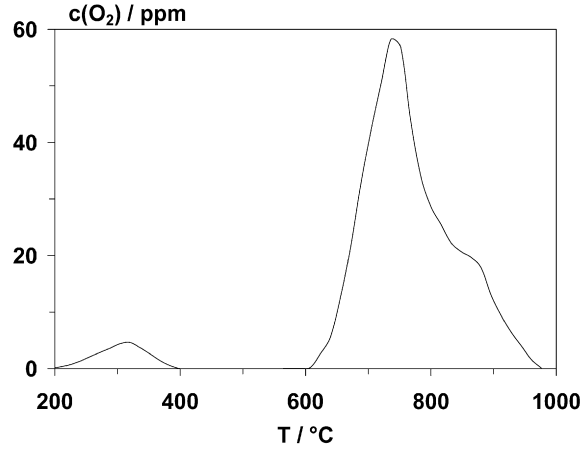

Fig. 1. O_2 TPD pattern of the Fe_2O_3 catalyst after exposure to O_2 at 200 °C. Conditions: $m = 15$ g, $F(N_2) = 500$ ml/min (STP), $\beta = 10$ K/min; catalyst is used in form of granules.

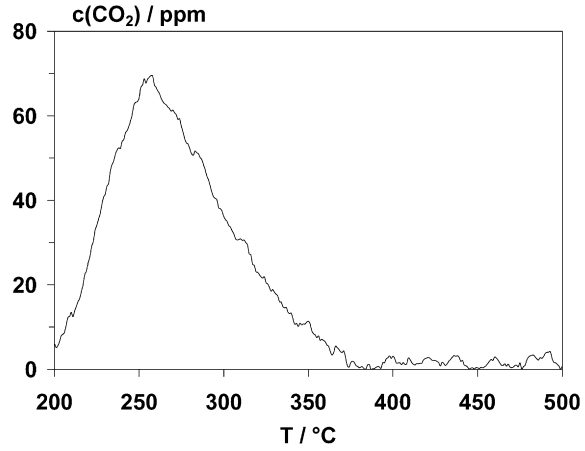

Fig. 2. CO_2 TPD pattern of the Fe_2O_3 catalyst after exposure to CO_2 at 200 °C. Conditions: $m = 1.6$ g, $F(N_2) = 500$ ml/min (STP), $\beta = 10$ K/min; catalyst is used in form of granules.

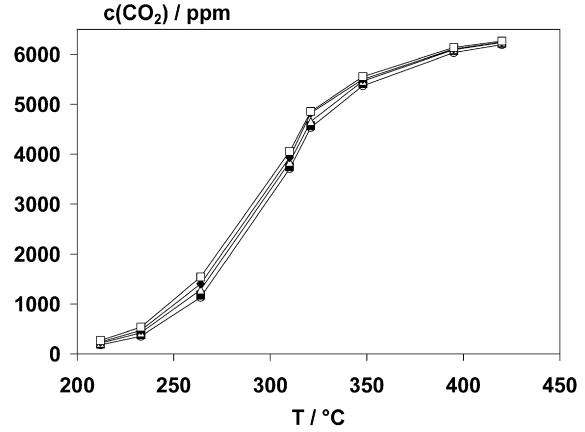

Fig. 3. Effect of O_2 on the formation of CO_2 in CO oxidation on the Fe_2O_3 catalyst (6.0 vol% O_2 (○), 25 vol% O_2 (■), 50 vol% O_2 (△), 75 vol% O_2 (◆), 99.3 vol% O_2 (□)). Conditions: $m = 500$ mg, $c(CO) = 7000$ ppm, $c(O_2) = 6.0$–99.3 vol%, N_2 balance, $F = 400$ ml/min (STP), SV = 10,000 h^{-1}, $\psi = 110$; catalyst is supported by a honeycomb.

with 25 vol% O_2, and was just 37% even with 99.3 vol%. But these measurements exclude a Langmuir–Hinshelwood type mechanism, which includes the adsorption of both reactants on the catalyst. The drastic increase in content of gaseous O_2 up to 99.3 vol%

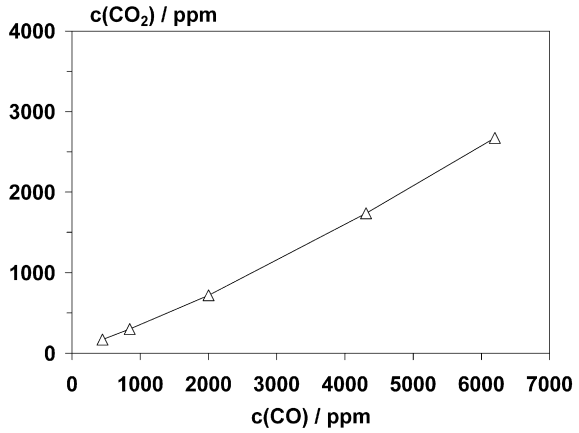

Fig. 4. Effect of CO on the formation of CO_2 on the Fe_2O_3 catalyst. Conditions: $m = 500$ mg, $T = 305\,^{\circ}C$, $c(CO) = 400$–6200 ppm, $c(O_2) = 6.0$ vol%, N_2 balance, $F = 400$ ml/min (STP), SV = 10,000 h^{-1}, $\psi = 110$; catalyst is supported by a honeycomb.

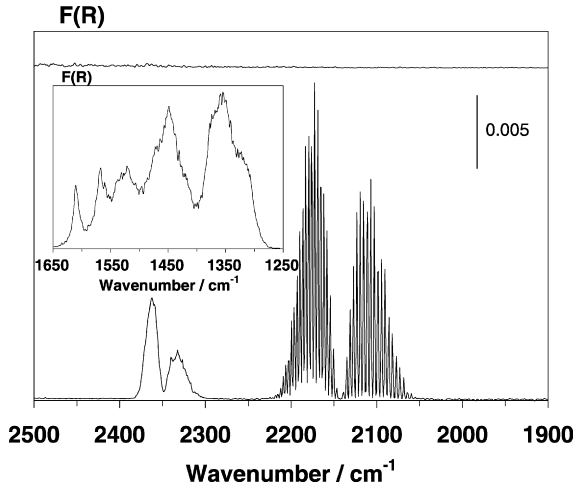

Fig. 5. In situ DRIFT spectrum of the Fe_2O_3 catalyst exposed at 200 °C to a mixture of 7000 ppm CO and 6.0 vol% O_2 balanced by N_2 (bottom and inset) and after subsequent flushing with N_2 at same temperature (top).

should then lead to a substantial decrease in CO oxidation due to displacement of CO from the surface.

Furthermore, the CO concentration varied from 400 to 6000 ppm for a fixed O_2 concentration of 6 vol% and a temperature of 305 °C. The corresponding results, depicted in Fig. 4, indicates increasing CO_2 production with increases in CO.

In the kinetic measurements the mass of carbon is always balanced; that is, the decrease in CO corresponds to the formation of CO_2. Thermodynamic data [30] show that complete CO conversion into CO_2 was allowed under the present conditions, providing evidence of kinetic restriction. Moreover, it should be noted that no oscillations in CO_2 concentration were observed in any of the experiments, as was reported for the CO oxidation on Pt catalysts [31].

In situ DRIFTS of CO oxidation on Fe_2O_3 performed at 200 °C revealed rotational vibrational bands of the gaseous educt CO (ν(CO), centred at 2143 cm^{-1}), and the gaseous product CO_2 ($\nu_{as}(CO_2)$, centred at 2349 cm^{-1}) (Fig. 5). No significant difference in the spectra recorded after 10 and 20 min was seen, indicating steady-state conditions. In addition, broad DRIFTS bands appeared between 1250 and 1650 cm^{-1} (inset of Fig. 5), associated mainly with CO_3^{2-} surface species coordinated to iron sites; some CO_2^- also formed [32,33]. The substantial presence of free carbonate is excluded, because it was derived from a careful analysis of the bands

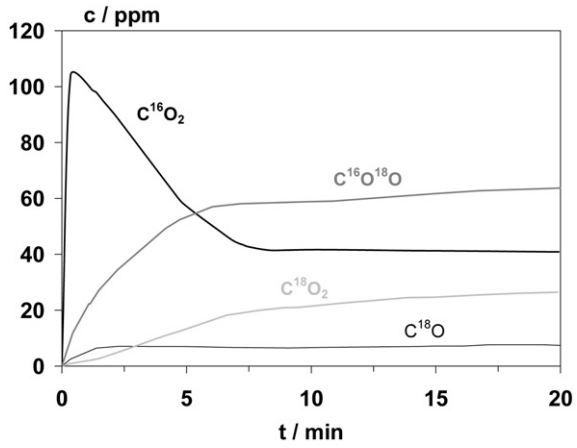

Fig. 6. CO oxidation on the Fe_2O_3 catalyst with $^{18}O_2$. Conditions: $m = 320$ mg, $T = 260\,^{\circ}C$, $c(CO) = 470$ ppm $C^{16}O$, $c(^{18}O_2) = 3000$ ppm, N_2 balance; catalyst is used in form of granules.

located at 1360 and 1450 cm^{-1}. In accordance with the literature, these features can be attributed to the $\nu_s(CO_2)$ and $\nu_{as}(CO_2)$ vibrations of monodentate carbonate complexes. The high intensity of the former band suggests that the corresponding absorbance at 1450 cm^{-1} refers mainly to the same surface species, ruling out the prominent presence of free carbonate ($\nu_{as}(CO_3^{2-})$), which would be expected at about 1450 cm^{-1} as well. This interpretation is in fair agreement with the findings of Davydov [33], who also noted the exclusive formation of coordinated carbonate on Fe_2O_3.

Moreover, no bands were detected that might be assigned to CO adsorbed on iron sites; these features would be expected in the range of 1990–2100 cm^{-1} [34], and thus they might be superimposed on the band of gaseous CO. But no specific band of adsorbed CO was found even after the gas-phase species was removed by flushing (Fig. 5). The same result was obtained when the sample was exposed to the CO/N_2 mixture for 10 min at 50 °C and at 200 °C, whereas carboxylate and carbonate surface compounds appeared. This is in line with the findings of Davydov [33] and Guglielminotti [34], who reported the absence of CO bands on oxidised Fe_2O_3 samples; corresponding features appeared only after drastic reduction and were related to CO coordinated to Fe^{2+} and Fe^0 sites [34]. Thus, it is obvious that in the present study, even exposure to the CO/N_2 mixture was not sufficient to achieve substantial reduction of the Fe_2O_3 catalyst surface. In contrast, CO was capable of reacting with the oxidised Fe_2O_3 surface to form CO_2^- and CO_3^{2-} species, as indicated earlier. Thus, these DRIFTS studies demonstrate that CO likely reacted from the gas phase with the surface oxygen species of the catalyst, without previous adsorption on Fe sites.

Oxidation of CO on the Fe_2O_3 catalyst also was evaluated using labeled gas-phase oxygen ($^{18}O_2$). The results of this isotopic study carried out at 260 °C, shown in Fig. 6, indicate rapid formation of $C^{16}O_2$ up to a maximum and then remaining at a constant level. Moreover, $C^{16}O^{18}O$ also was produced immediately and become the major product after ca. 6 min, whereas $C^{18}O_2$ formation required a certain latency period. In addition, $C^{18}O$ was detected in minor amounts. Finally, all CO_x species recorded reached a steady-state concentration. This feature is characterized as the exchange of gas-phase and surface oxygen by the surface carbonate species; that is, in the adsorption/desorption equilibrium, CO_2 reacts with surface oxygen to yield carbonate complexes, and then in subsequent desorption, one original oxygen of the CO_2 remains on the surface, and the original surface oxygen desorbs as CO_2 [35,36]. Fig. 6 shows that in the beginning of the catalytic conversion, CO reacted with surface oxygen of the iron oxide to form $C^{16}O_2$

(Eq. (1)). With increasing reaction time, the surface oxygen (^{16}O) released was refilled by gas phase $^{18}O_2$ (Eq. (2)), with * representing oxygen vacancy, thereby leading to the major production of $C^{16}O^{18}O$ (Eq. (3)). This implies the successive substitution of the initial surface oxygen by gas-phase oxygen. Based on the trace of $C^{16}O_2$ the amount of surface oxygen involved in CO oxidation is roughly estimated to be 0.87 μmol/m^2. This quantity, stated as atomic O, is close to the abundance of oxygen released in O_2 TPD. Furthermore, the production of $C^{18}O_2$ was related mainly to the mentioned oxygen exchange on the Fe_2O_3 surface (Eq. (4)), with the conversion of $C^{18}O$ with surface ^{18}O possibly contributing to a minor extent (Eq. (5)). The low formation of $C^{18}O$ might be ascribed to the exchange of oxygen in the adsorption/desorption of CO (Eq. (6)); however, the contribution of adsorbed CO to the formation of CO_2 is assumed to be negligible, as discussed below. We also note that for simplicity, $C^{16}O$ is not shown in Fig. 6, implying a balanced mass of C, as stated above:

$$C^{16}O(g) + {}^{16}O_{ads} \rightarrow C^{16}O_2(g) + *, \tag{1}$$

$$0.5\,{}^{18}O_2(g) + * \rightarrow {}^{18}O_{ads}, \tag{2}$$

$${}^{18}O_{ads} + C^{16}O(g) \rightarrow C^{16}O^{18}O(g) + *, \tag{3}$$

$${}^{18}O_{ads} + C^{16}O^{18}O(g) \rightarrow C^{18}O_2(g) + {}^{16}O_{ads}, \tag{4}$$

$$C^{18}O(g) + {}^{18}O_{ads} \rightarrow C^{18}O_2(g) + *, \tag{5}$$

$$C^{16}O(g) + {}^{18}O_{ads} \rightarrow C^{18}O(g) + {}^{16}O_{ads}. \tag{6}$$

The findings of our DRIFTS, isotopic, and kinetic studies suggest that the CO oxidation on the Fe_2O_3 catalyst followed an Eley–Rideal type mechanism. This route involves the dissociative adsorption of O_2 on the catalyst, in agreement with the literature [37]. The surface oxygen species thus formed then react with gas-phase CO, producing CO_2. The model of this Eley–Rideal type mechanism is in line with that of Renken et al. [38], who reported the CO oxidation by a Fe_2O_3/SiO_2 catalyst in the absence of O_2. Furthermore, quantum mechanical calculations from Kandalam et al. indicate that on the (100) surface, CO oxidation on nanosized Fe_2O_3 occurs through an Eley–Rideal mechanism, whereas on the (0001) plane, a Langmuir–Hinshelwood type mechanism contributes [38]. Despite the aforementioned arguments for Eley–Rideal type mechanism, we must note that, particularly for CO oxidation, the Langmuir–Hinshelwood mechanism is considered kinetically favoured from a fundamental standpoint [39]. A possible explanation for this apparent contradiction might be the extremely low coverage of the active Fe sites by CO, as demonstrated by the aforementioned DRIFTS studies, demonstrating a preference for the Eley–Rideal type route.

3.3. Kinetic modeling

The postulated Eley–Rideal type mechanism of the CO oxidation on Fe_2O_3 catalyst is described by the reaction scheme defined by Eqs. (7)–(9). This network involves 2 surface species, 3 gas-phase species and 6 elementary reactions. As mentioned above the asterisk (*) labels a free iron site characterised by a surface vacancy that is generally accepted to act as an active species [40,41]:

$$O_2(g) + 2* \underset{r_2}{\overset{r_1}{\leftrightarrows}} 2O*, \tag{7}$$

$$CO(g) + O* \underset{r_4}{\overset{r_3}{\leftrightarrows}} CO_2^*, \tag{8}$$

$$CO_2(g) + * \underset{r_6}{\overset{r_5}{\leftrightarrows}} CO_2^*. \tag{9}$$

Reactions (7) and (9) represent the adsorption/desorption equilibrium of O_2 and CO_2, respectively, whereas reaction (8) implies the formation of CO_2. The DRIFTS studies show the production of carbonate species coordinating to Fe sites. Such surface complexes are formed by interaction of CO_2 with surface oxygen in close proximity to Fe sites. But Eq. (9) does not differentiate these surface carbonates from CO_2, which adsorbs on the Fe sites without forming carbonates. The present kinetic model is based on the mean field approximation; that is, the different types of active iron sites are supposed to be equal.

For every forward and backward reaction, an Arrhenius based rate expression is used (Eqs. (10)–(15)), where A_i is the preexponential factor, E_i is the activation energy, $E_i(0)$ is the activation energy at zero coverage, c_i is the gas-phase concentration of species i, θ_i is the respective coverage, and θ_* is the relative number of free Fe sites. Due to repulsion of adsorbed species, a linear decrease in activation energy with increasing oxygen coverage is assumed for the desorption of O_2 (Eq. (11)) and CO_2 (Eq. (15)); for this purpose, the constant α_j is introduced. However, as known for Pt [16], it is supposed that the dissociation of CO_2 (Eq. (13)) is inhibited by oxygen, and thus an increase in activation energy with increasing O coverage is taken into account:

$$r_1 = A_1 \exp\left(-\frac{E_1}{RT}\right) c_{O_2} \theta_*^2, \tag{10}$$

$$r_2 = A_2 \exp\left(-\frac{E_2(0) - \alpha_2 \theta_o}{RT}\right) \theta_O^2, \tag{11}$$

$$r_3 = A_3 \exp\left(-\frac{E_3}{RT}\right) c_{CO} \theta_O, \tag{12}$$

$$r_4 = A_4 \exp\left(-\frac{E_4(0) + \alpha_4 \theta_O}{RT}\right) \theta_{CO_2}, \tag{13}$$

$$r_5 = A_5 \exp\left(-\frac{E_5}{RT}\right) c_{CO_2} \theta_*, \tag{14}$$

$$r_6 = A_6 \exp\left(-\frac{E_6(0) - \alpha_6 \theta_O}{RT}\right) \theta_{CO_2}. \tag{15}$$

For modeling of the CO oxidation and determination of the surface coverage, some kinetic parameters were taken from the literature and others were calculated, to reduce the number of free parameters in the fitting procedure. The numeric modeling was based on a combination of the mass balance of each gas phase (Eq. (16)) and adsorbed species (Eq. (17)). Because CO surface species were neglected, a system of five algebraic equations was obtained, where F denotes the flow rate, ν_{ij} is the respective stoichiometric coefficient, A_{act} is the surface of the Fe_2O_3 catalyst and Γ_{cat} is the surface concentration of active sites. The steady-state surface coverages for the CO oxidation in the loop reactor were calculated using the Matlab tool lsqnonlin. The temperature-dependent surface coverages were calculated using the Matlab tool ode15s, whereas the free parameters were simulated with the Matlab tool lsqurvefit (nonlinear regression):

$$F c_{i,in} - F c_{i,out} + A_{act} \sum_j^{N_j} \nu_{ij} r_{ij} = 0, \tag{16}$$

$$0 = A_{act} \sum_j^{N_j} \nu_{ij} r_{ij}. \tag{17}$$

The preexponential factor for the adsorption of O_2 (A_1) and CO_2 (A_5) was calculated using Eq. (18), which was derived from the kinetic gas theory [42,43], where N_A is the Avogadro number, R is the molar gas constant, M_i is the molar mass of the gas species, a_m is the surface area per Fe site, Γ_{cat} is the surface concentration of the active Fe sites, and S^0 is the sticking coefficient for zero

coverage. In the calculations, the temperature dependency was neglected by using an average temperature of 1073 K for O_2 and 573 °C for CO_2; these temperatures refer to the specific TPD profile.

For oxygen, S^0 was assumed to be 0.09, as reported for an oxidised Fe(111) surface by Arabczyk et al. [44,45]. Furthermore, a_m was assumed to be 2.0×10^{-20} m^2 per site, as deduced from the radius of the Fe^{3+} cation (7.9×10^{-11} m) [44]. Γ_{cat} was determined by multiplying N_A by the surface concentration of Fe sites of the (0001) and (1120) planes of α-Fe_2O_3 averaged as 3.7×10^{18} sites/m^2 [40]. This calculation resulted in a site concentration of 6.2 μmol/m^2, which is in the range of the values found in the isotopic study (0.87 μmol/m^2) and O_2 TPD (0.16 μmol/m^2), indicating a realistic estimation. Finally, by Eq. (18), A_1 was found to be 1.4 m/s:

$$A_i = \frac{N_A RT}{(2\pi M_i RT)^{1/2}} a_m \Gamma_{cat} S^0. \tag{18}$$

For the calculation of A_5 the sticking coefficient of CO_2 was estimated according to the procedure outlined in Section 2.6, leading to 0.061 ± 0.010. This value is close to the sticking coefficients of CO_2 on Pt (0.005 [45]) and of O_2 on Fe_2O_3 (0.09 [40]) and thus should be more realistic than the data reported for elemental Fe, indicating 10^{-7} [46]. Note also that the assumed surface concentration of Fe sites (6.2 μmol/m^2) is slightly higher than the amount of CO_2 released in TPD (0.68 μmol/m^2). Consequently, A_5 was calculated to be 0.74 m/s.

Furthermore, the activation energy for the adsorption of O_2 and CO_2 was neglected (i.e., $E_1 = E_5 = 0$ kJ/mol), which is in good agreement with the findings for related solid–gas systems [47,48].

To obtain independent kinetic parameters for the adsorption and desorption of oxygen and carbon dioxide, the patterns of O_2 TPD and CO_2 TPD were modeled numerically. The approach was the same as that described above for CO oxidation, with the respective mass balance of the adsorbed and gaseous species resulting in a system of one algebraic equation and one nonlinear differential equation. The corresponding equations are exemplified for O_2 [Eqs. (19)–(22)], with the temperature-dependent surface coverages calculated using Matlab tool ode15s:

$$F c_{O_2(g),in} - F c_{O_2(g),out} - A_{act} r_1 + A_{act} r_2 = 0, \tag{19}$$

$$A_{act} \Gamma_{cat} \frac{d\theta_O}{dt} = 2A_{act} r_1 - 2A_{act} r_2, \tag{20}$$

$$c_{O_2(g)} = \frac{A_{act} A_2 \exp(-\frac{E_2(0) - \alpha_2 \theta_O}{RT}) \theta_O^2}{F + A_{act} A_1 \exp(-\frac{E_1}{RT}) \theta_*^2}, \tag{21}$$

$$A_{act} \Gamma_{cat} \beta \frac{d\theta_O}{dT} = 2A_{act} A_1 \exp\left(-\frac{E_1}{RT}\right) c_{O_2(g)} \theta_*^2 - 2A_{act} A_2 \exp\left(-\frac{E_2(0) - \alpha_2 \theta_O}{RT}\right) \theta_O^2. \tag{22}$$

It is worth mentioning that Eq. (19) describes the plug flow reactor (PFR) used for TPD using the model for the continuously stirred tank reactor; that is, the differential term of the PFR is neglected assuming stationary conditions. This approach has been shown to be a fair approximation in TPD modeling and is frequently applied [48–50].

In the estimation procedure, the preexponential factor (A_1 or A_5) and the activation energy of adsorption (E_1 or E_5) are kept fixed, while the remaining parameters are fitted, i.e. A_2, E_2 and α_2 for O_2 TPD and A_6, E_6 and α_6 for CO_2 TPD. For O_2 TPD the fit leads to an activation energy for O_2 desorption of 193 kJ/mol, whereas A_2 is calculated to be 3×10^{10} mol/(s m^2) and α_2 to 1.6×10^{-3} kJ/mol. The activation energy for O_2 desorption is close to that on Pt which is reported to be 200 kJ/mol [51] and 213 kJ/mol [52], respectively. However, α_2 is significantly lower than for Pt (20 kJ/mol) [42,51]. This low value α_2 can be interpreted with the weak repulsion of the O surface species and/or a rather homogeneous Fe_2O_3 surface [48]. The first feature might be associated with the relatively low surface concentration of the active Fe sites (6.2 μmol/m^2) as compared to Pt thus leading to larger average distance of the surface oxygen species; for comparison Γ_{cat} is reported to be approx. 26 μmol/m^2 for Pt catalysts [51]. Additionally, the rather low surface area of the Fe_2O_3 catalyst (15 m^2/g) supports the argument of homogeneous surface. Fig. 7 shows that the O_2 TPD profile is well described by the kinetic data implemented in the O_2 adsorption/desorption model. As a consequence of the mean field model, the TPD pattern is approximated by one peak only. The profile of the Fe_2O_3 coverage is depicted in the inset of Fig. 7 indicating that the coverage is high in the beginning of TPD and decreases continuously with temperature.

Furthermore, Fig. 8 shows that the CO_2 TPD is satisfactorily fitted as well. The profile of the Fe_2O_3 coverage illustrated in the inset demonstrates high initial coverage rapidly declining to zero, i.e. already at ca. 320 °C CO_2 is completely removed from the Fe_2O_3 surface. The calculations provide an activation energy for CO_2 desorption (E_6) of 99 kJ/mol, while A_6 is 8×10^6 mol/(s m^2) and α_6 is 1 kJ/mol. E_6 is consistent with the result from Renken et

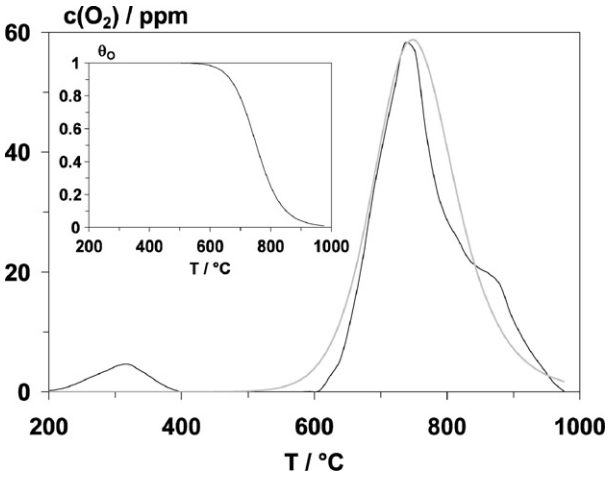

Fig. 7. Experimental (—) and fitted O_2 TPD pattern (—) of the Fe_2O_3 catalyst. The inset shows the calculated Fe_2O_3 coverage by O_2. Conditions: $m = 15$ g, $F(N_2) = 500$ ml/min (STP), $\beta = 10$ K/min; catalyst is used in form of granules and preliminary O_2 exposure is at 200 °C.

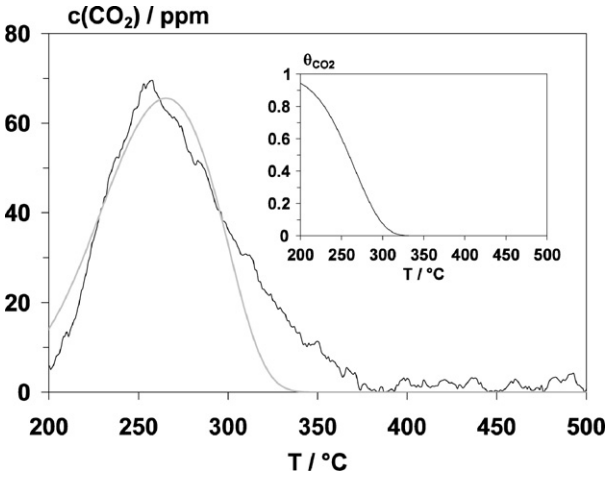

Fig. 8. Experimental (—) and fitted CO_2 TPD pattern (—) of the Fe_2O_3 catalyst. The inset shows the calculated Fe_2O_3 coverage by CO_2. Conditions: $m = 1.6$ g, $F(N_2) = 500$ ml/min (STP), $\beta = 10$ K/min; catalyst is used in form of granules and preliminary CO_2 exposure is at 200 °C.

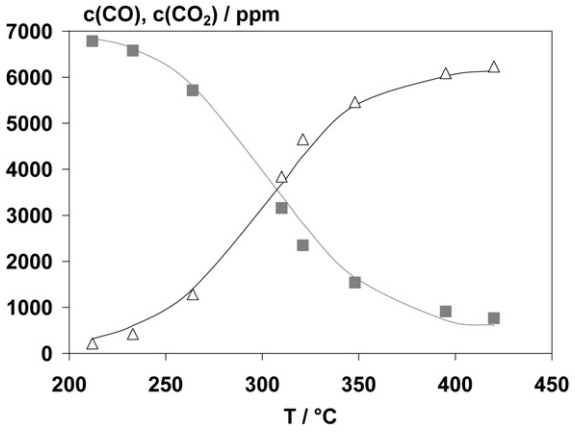

Fig. 9. Comparison of experimental CO (■) and CO_2 concentration (△) with the fitted data (corresponding curves) in CO oxidation on the Fe_2O_3 catalyst. Conditions: $m = 500$ mg, $c(CO) = 7000$ ppm, $c(O_2) = 50$ vol%, N_2 balance, $F = 400$ ml/min (STP), SV = 10,000 h^{-1}, $\psi = 110$; catalyst is supported by a honeycomb.

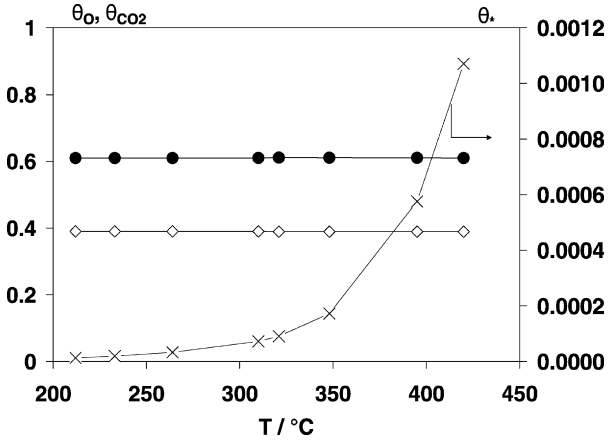

Fig. 10. Calculated Fe_2O_3 coverage in CO oxidation of the Fe_2O_3 catalyst; θ_O (●), θ_{CO_2} (◇), θ_* (×). The experimental conditions are presented in Fig. 9.

Table 1
Kinetic parameters of the CO oxidation on the Fe_2O_3 catalyst.

Parameter	Value	Tolerance[a]	Unit	Reference
A_1	1.4		m/s	Calculated[b]
E_1	0		kJ/mol	[51]
A_2	3×10^{10}	$\pm 1 \times 10^{7}$	mol/(s m^2)	Derived from O_2 TPD
E_2	192.7	±1.25	kJ/mol	Derived from O_2 TPD
α_2	1.55×10^{-3}	$\pm 0.8 \times 10^{-3}$	kJ/mol	Derived from O_2 TPD
A_3	1.0×10^{3}	$\pm 1.8 \times 10^{-2}$	mol/(s m^2)	Numerical fit
E_3	97.0	±0.2	kJ/mol	Numerical fit
A_4	4.0×10^{7}	$\pm 1.2 \times 10^{2}$	mol/(s m^2)	Numerical fit
E_4	185.5	±0.02	kJ/mol	Numerical fit
α_4	1.0	$\pm 3.8 \times 10^{-2}$	kJ/mol	Numerical fit
A_5	0.74		m/s	Calculated[b]
E_5	0		kJ/mol	[50,51]
A_6	1.3×10^{4}		mol/(s m^2)	Numerical fit
E_6	98.5	±1.01	kJ/mol	Derived from CO_2 TPD
α_6	1	±0.12	kJ/mol	Derived from CO_2 TPD

[a] 95% confidence interval.
[b] Calculated with Eq. (18).

al. reporting 88 kJ/mol for a Fe_2O_3/SiO_2 catalyst [23]. However, these activation energies are significantly higher than for Pt [51] that might be attributed to the stabilisation of CO_2 by carbonate complexes formed on the oxide surface.

For the modeling of the CO oxidation, the kinetic parameters obtained from the TPD calculations are taken. An exception is A_6 that is used as variable to implement the interaction between adsorbed CO_2 and O_2 in the kinetic parameters of CO_2 adsorption/desorption. Thus, in the estimation procedure A_3, E_3, A_4, E_4, α_4 and A_6 are fitted. For the fit procedure the experimental data obtained with 7000 ppm CO and 50 vol% O_2 are used. Fig. 9 evidences that the calculated CO and CO_2 concentrations correspond well with the measured results. The maximum difference of calculated and experimental data is about 3%. The kinetic parameters used are demonstrated in Table 1 along with the respective 95% confidence interval substantiating the reliability of the calculations. Furthermore, this table shows an activation energy for the CO_2 formation (E_3) of 96 kJ/mol being close to that of Pt (108 kJ/mol) [18,45]. Contrary, Renken et al. report on a slightly lower activation energy (75 kJ/mol) that is consistent with their lower value of the activation energy for CO_2 desorption [23]; this may refer to activation of Fe_2O_3 by the SiO_2 support. In addition, in agreement with α_2 and α_6 the value of α_4 is very low (1×10^{-2} kJ/mol). Furthermore, in the numeric modeling of the CO oxidation a lower preexponential factor for CO_2 desorption (A_6) is obtained than in CO_2 TPD. This might be related to the repulsive interaction of adsorbed CO_2 with surface oxygen accelerating the desorption. The calculation of the Fe_2O_3 coverage indicates that the adsorbed oxygen dominates the surface in the entire temperature regime (Fig. 10). In contrast to that, the amount of free Fe sites is extremely low.

Finally, based on the determined kinetic parameters the rate determining step of the CO oxidation on the Fe_2O_3 catalyst is discussed. As the adsorption of O_2 is considered to be an unactivated process and the increase in gas phase concentration does not lead to a drastic increase in CO conversion this reaction is not accounted for the limiting factor. This is also supported by the calculated Fe_2O_3 coverage showing high proportion of surface oxygen species. Moreover, while the activation energy for CO_2 formation (E_3) is quite similar to that of CO_2 desorption (E_6) the preexponential factor of the latter (A_6) is one order of magnitude higher than A_3. Present comparison suggests that the formation of CO_2, i.e. the reaction of gaseous CO with the active surface oxygen, represents the limiting step of the overall reaction. This is additionally substantiated by the fact that the experimental CO_2 formation is well described just by the rate expression r_3, whereas with r_1 and r_6 higher rates are obtained: For instance, the experimental CO_2 production rate at 265 °C is ca. 10^{-7} mol/s for 7000 ppm CO and 50 vol% O_2, while with r_3 it is estimated to be 10^{-7} mol/s as well; r_1 and r_6 provide clearly faster rates, i.e. 10^{-2} and 10^{-6} mol/s.

3.4. Model validation

For validation of the kinetic model the experiments are simulated in which the concentration of O_2 (Fig. 11), CO (Fig. 12) or CO_2 (Fig. 13) is varied. The simulations are performed based on Eqs. (16) and (17) using the respective experimental conditions as well as the kinetic parameters presented in Table 1. As mentioned for the TPD calculations, the CO_2 variation studies carried out in the PFR are simulated by employing the CSTR model. Figs. 11 to 13 show that all the experimental data are well described by the simulations. The maximum difference is obtained in the CO variation amounting to 15% only indicating the accuracy of the simulations. Hence, the model validation evidences the relevance of the constructed kinetic model for a broad range of experimental conditions.

3.5. Thermodynamic consistency

To check the thermodynamic consistency of the kinetic parameters of the established model the approach from Mhadeshwar et al. is taken into consideration [53]. According to this, the relation

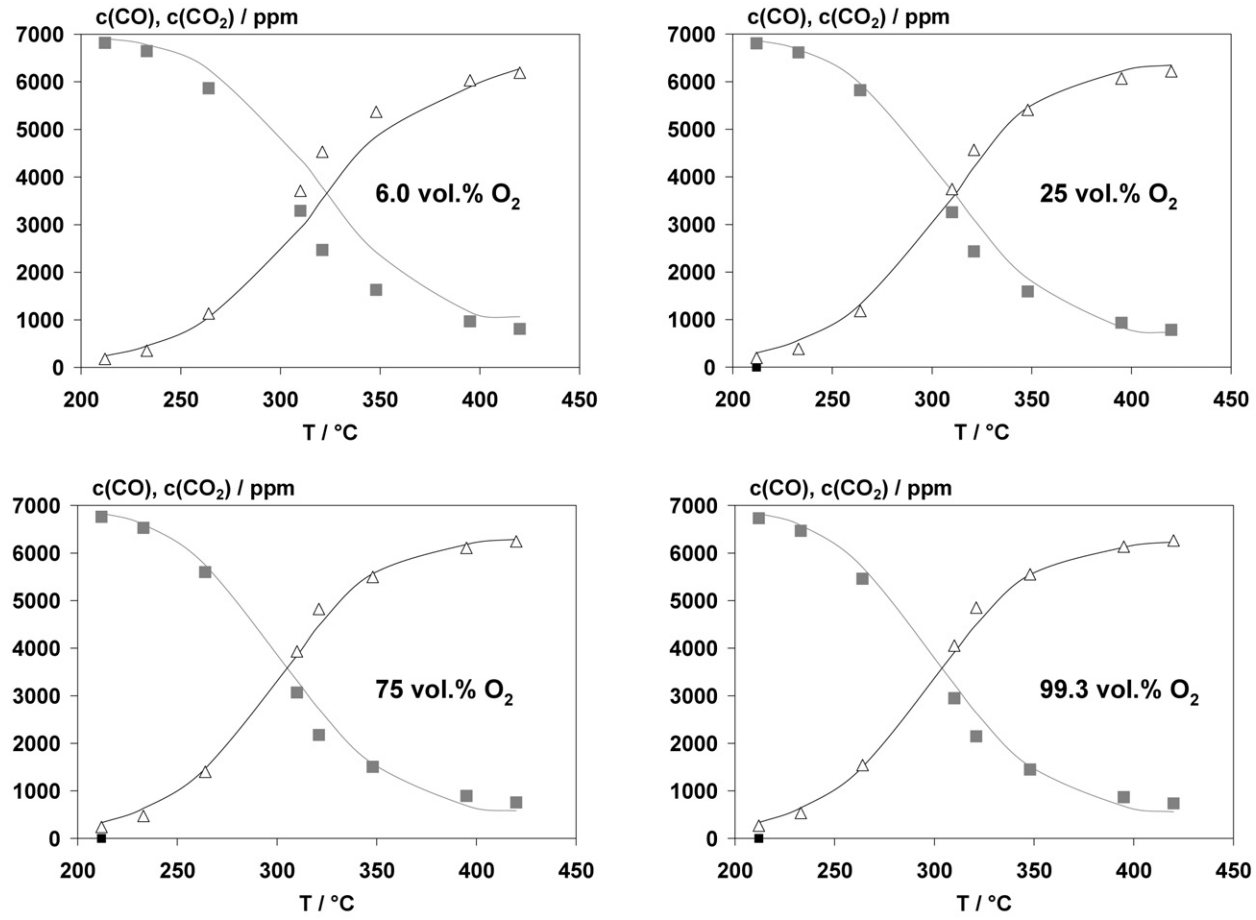

Fig. 11. Comparison of CO (■) and CO_2 concentration (△) with simulated data (corresponding curves) in CO oxidation on the Fe_2O_3 catalyst. Conditions: $m = 500$ mg, $c(CO) = 7000$ ppm, $c(O_2) = 6.0$–99.3 vol%, N_2 balance, $F = 400$ ml/min (STP), SV = 10,000 h^{-1}, $\psi = 110$; catalyst is supported by a honeycomb.

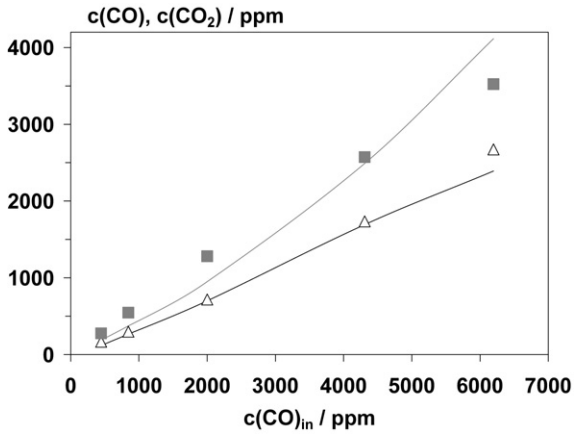

Fig. 12. Experimental and simulated concentration of CO (■) and CO_2 (△) in CO oxidation on the Fe_2O_3 catalyst; the simulated data are the corresponding curves. Conditions: $m = 500$ mg, $c(CO) = 400$–6190 ppm, $c(O_2) = 6.0$ vol%, N_2 balance, $F = 400$ ml/min (STP), SV = 10,000 h^{-1}, $\psi = 110$; catalyst is supported by a honeycomb.

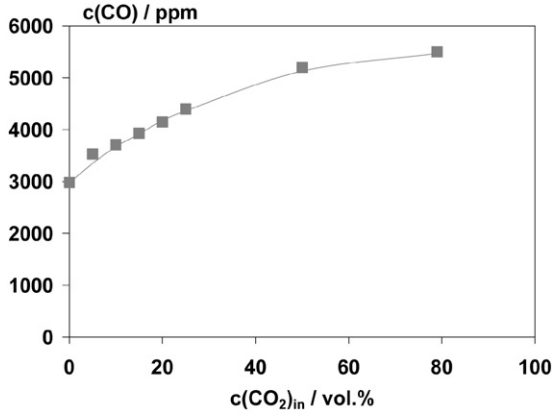

Fig. 13. Comparison of experimental CO concentration (■) with simulated data (curve) in CO oxidation on the Fe_2O_3 catalyst. Conditions: $m = 500$ mg, $c(CO) = 7000$ ppm, $c(O_2) = 20$ vol%, $c(CO_2) = 0$–79.3 vol%, N_2 balance, $F = 500$ ml/min (STP), SV = 13,000 h^{-1}; catalyst is supported by a honeycomb and the measurements are performed in the plug flow reactor (Section 2.3).

of enthalpy and entropy with activation energy and preexponential factor of a given reaction (i) implying forward (f) and backward reaction (b) is defined as follows:

$$\Delta H_i = E_i^{\mathrm{f}} - E_i^{\mathrm{b}}, \tag{23}$$

$$\frac{A_i^{\mathrm{f}}}{A_i^{\mathrm{b}}} = \exp\left(\frac{\Delta S_i}{R}\right). \tag{24}$$

For the gas phase reaction $CO(g) + 0.5O_2(g) \rightarrow CO_2(g)$ the enthalpy and entropy are calculated based on Eqs. (25) and (26):

$$\Delta H = H^0_{\mathrm{f,CO_2}} + \int_{T^0}^{\bar{T}} c_{\mathrm{p,CO_2}} dT - \left(H^0_{\mathrm{f,CO}} + \int_{T^0}^{\bar{T}} c_{\mathrm{p,CO}} dT\right) - \frac{1}{2}\left(H^0_{\mathrm{f,O_2}} + \int_{T^0}^{\bar{T}} c_{\mathrm{p,O_2}} dT\right), \tag{25}$$

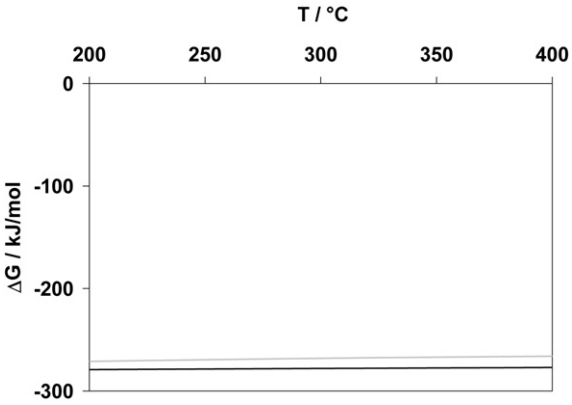

Fig. 14. Comparison of the Gibbs free enthalpy of the gas phase (—) and catalytic reaction (—) derived from kinetic parameters according to Eqs. (25)–(28).

$$\Delta S = \frac{1}{R}\left[\left(S^0_{CO_2} + \int_{T^0}^{\bar{T}} c_{p,CO_2}\frac{dT}{T}\right) - \left(S^0_{CO} + \int_{T^0}^{\bar{T}} c_{p,CO}\frac{dT}{T}\right) - \frac{1}{2}\left(S^0_{O_2} + \int_{T^0}^{\bar{T}} c_{p,O_2}\frac{dT}{T}\right)\right]. \quad (26)$$

Combination of Eqs. (23) and (24) with the corresponding kinetic parameters leads to the following equations:

$$\Delta H = \frac{1}{2}(E_1 - E_2) + (E_3 - E_4) + (E_5 - E_6), \quad (27)$$

$$\Delta S = \ln\left(\left(\frac{A_1}{A_2}\right)^{1/2} \cdot \left(\frac{A_3}{A_4}\right) \cdot \left(\frac{A_5}{A_6}\right)\right). \quad (28)$$

For the average temperature of 325 °C the enthalpy and entropy is calculated for the gas phase reaction to be −285 kJ/mol and −11 J/(mol K), respectively. By using the kinetic parameters according to Eqs. (27) and (28) the enthalpy is −283 kJ/mol and the entropy −26 J/(mol K). These results are close to the data obtained for the gas phase reaction. Although a slight difference remains, this error is considered to be acceptable being in line with the discussions of Mhadeshwar et al. [53]. Thus, we derive thermodynamic consistency of the kinetic parameters. This conclusion is substantiated by the Gibbs free enthalpy showing a minor difference between gas phase and catalytic reaction only amounting to ca. 4% in the whole temperature range (Fig. 14).

4. Conclusion

From in situ DRIFT spectroscopic examinations, isotopic labeling and kinetic studies carried out in a gradient-free loop reactor, we have deduced an Eley–Rideal type mechanism for CO oxidation on the model catalyst α-Fe_2O_3. This route includes dissociative adsorption of O_2, followed by reaction with gas-phase CO to form CO_2, in fair agreement with literature reports. Based on the mechanistic and kinetic examinations, a mean field model was developed that includes a network of six elementary reactions, that is, the adsorption/desorption of O_2 and CO_2 as well as the formation and dissociation of CO_2 on the catalyst surface. Whereas the preexponential factor of the adsorption of O_2 and CO_2 was derived from the kinetic gas theory, the adsorption of these components was assumed to be unactivated; that is, the respective activation energy was zero. In addition, the CO_2 and O_2 TPD patterns were numerically modeled to reduce the number of free parameters in the fit procedure, whereby independent kinetic parameters are obtained. The remaining kinetic parameters were estimated by numerically modeling the experimental data of the CO oxidation. Using this set of kinetic parameters, a series of simulations was performed, including variations in temperature as well as in CO, O_2, and CO_2 concentrations. As a result of the model validation, all of the simulations covered the experimental data well, demonstrating the reliability of the kinetic model. Finally, the reaction of surface oxygen species with gaseous CO was found to be the rate-determining step of the present catalytic process, and the kinetic parameters were found to be thermodynamically consistent.

References

[1] R.P. Wayne, Chemistry of Atmospheres: An Introduction to the Chemistry of the Atmospheres of Earth, the Plants and Their Satellites, Oxford Univ. Press, Oxford, 2000.
[2] P. Zelenka, W. Cartellieri, P. Herzog, Appl. Catal. B 7 (1996) 3.
[3] M.V. Twigg, Appl. Catal. B 70 (2007) 2.
[4] O. Salvat, P. Marez, G. Belot, SAE Paper 2000-01-0473.
[5] J. Van Doorn, J. Varloud, P. Meriaudeau, V. Perrichon, Appl. Catal. B 1 (1992) 117.
[6] B.J. Cooper, J.E. Thoss, SAE paper 890404.
[7] F. Jacquot, V. Logie, J.F. Brilhac, P. Gillot, Carbon 40 (2002) 335.
[8] M. Guyon, P. Blanche, C. Bert, L. Philippe, I. Messaoudi, SAE Paper 2000-01-2910.
[9] I. Nova, L. Castoldi, L. Lietti, E. Tronconi, P. Forzatti, F. Prinetto, G. Ghiotti, J. Catal. 222 (2004) 377.
[10] L. Olsson, E. Fridell, M. Skoglundh, B. Andersson, Catal. Today 72 (2002) 263.
[11] F. Rohr, S.D. Peter, E. Lox, M. Kögel, A. Sassi, L. Juste, C. Rigaudeau, G. Belot, P. Gelin, M. Primet, Appl. Catal. B 56 (2005) 201.
[12] G. Busca, L. Lietti, G. Ramis, F. Berti, Appl. Catal. B 18 (1998) 1.
[13] N.Y. Topsøe, H. Topsøe, J.A. Dumesic, J. Catal. 151 (1995) 226.
[14] A.Z. Ma, W. Grünert, Chem. Commun. 1 (1999) 71.
[15] R.Q. Long, R.T. Yang, J. Catal. 188 (1999) 332.
[16] D. Chatterjee, O. Deutschmann, J. Warnatz, Faraday Discuss. 119 (2001) 371.
[17] D.K. Zerkle, M.D. Allendorf, M. Wolf, O. Deutschmann, J. Catal. 196 (2000) 18.
[18] C.T. Campbell, G. Ertl, H. Kuipers, J. Segner, J. Chem. Phys. 73 (1980) 5862.
[19] M. Bandyopadhyay, O. Korsak, M.W.E. van den Berg, W. Grünert, A. Birkner, W. Li, F. Schüth, H. Gies, Microporous Mesoporous Mater. 89 (2006) 158.
[20] R.J.H. Voorhoeve, J.P. Remeika, L.E. Trimble, Ann. N.Y. Acad. Sci. 272 (1976) 3.
[21] R. Zhang, H. Alamdari, S. Kaliaguine, J. Catal. 242 (2006) 241.
[22] G.A. Fagal, G.A. El-Shobaky, S.M. El-Khouly, Colloids Surf. A 178 (2001) 287.
[23] H. Randall, R. Doepper, A. Renken, Ind. Eng. Chem. Res. 36 (1997) 2996.
[24] M.J. Kahlich, H.A. Gasteiger, R.J. Behm, J. Catal. 182 (1999) 430.
[25] T. Schalow, B. Brandt, M. Laurin, S. Schauermann, J. Libuda, H.-J. Freund, J. Catal. 242 (2006) 58.
[26] S. Kureti, W. Weisweiler, K. Hizbullah, Appl. Catal. B 43 (2003) 281.
[27] D.E. Mears, Ind. Eng. Chem. Process. Des. Dev. 10 (1971) 541.
[28] P.W. Atkins, Physical Chemistry, Oxford Univ. Press, Oxford, 1986.
[29] E.E. Unmuth, L.H. Schwartz, J.B. Butt, J. Catal. 61 (1980) 242.
[30] D.R. Lide (Ed.), Handbook of Chemistry and Physics, 74th ed., CRC Press, Boca Raton, 1994.
[31] L.F. Razon, R.A. Schmitz, Catal. Rev.-Sci. Eng. 28 (1986) 89.
[32] K. Nakamoto, Infrared and Raman Spectra of Inorganic and Coordination Compounds, Part B, Wiley, New York, 1997.
[33] A.A. Davydov, Infrared Spectroscopy of Adsorbed Species on the Surface of Transition Metal Oxides, Wiley, New York, 1990.
[34] E. Guglielminotti, J. Phys. Chem. 98 (1994) 4884.
[35] J. Novakova, Catal. Rev. 4 (1970) 77.
[36] K. Sakata, F. Ueda, M. Misono, Y. Yoneda, Bull. Chem. Soc. Jpn. 53 (1980) 324.
[37] E.M. Jarvis, A.M. Chaka, Surf. Sci. 601 (2007) 1909.
[38] A.K. Kandalam, B. Chatterjee, S.N. Khanna, B.K. Rao, P. Jena, B.V. Reddy, Surf. Sci. 601 (2007) 4873.
[39] C.B. Mullins, W.H. Weinberg, in: G. Ertl, H. Knoezinger, J. Weitkamp (Eds.), Handbook of Heterogeneous Catalysis, vol. 3, first ed., Wiley–VCH, New York, 1997, p. 972.
[40] M. Iwamoto, Y. Yoda, N. Yamazoe, T. Seiyama, Bull. Chem. Soc. Jpn. 51 (1978) 2765.
[41] M. Iwamoto, Y. Yoda, N. Yamazoe, T. Seiyama, J. Phys. Chem. 82 (1978) 2564.
[42] L. Olsson, B. Westerberg, H. Persson, E. Fridell, M. Skoglundh, B. Andersson, J. Phys. Chem. B 103 (1999) 10433.
[43] K. Christmann, Introduction to Surface Physical Chemistry, Springer, New York, 1991.
[44] R.D. Shannon, C.T. Prewitt, Acta Crystallogr. B 25 (1969) 925.
[45] O. Deutschmann, Habilitation thesis, University of Heidelberg, 2001.

[46] B. Langenbeck, F.J. Schittko, Adv. Vac. Sci. Technol. Proc. 3rd Int. Congr. (1966) 487.
[47] D. Chatterjee, T. Burkhardt, M. Weibel, I. Nova, A. Grossale, E. Tronconi, SAE paper 2007-01-1136.
[48] T. Finke, M. Hartmann, M. Gernsbeck, U. Eisele, C. Vincent, S. Kureti, H. Bockhorn, Thermochim. Acta 473 (2008) 32.
[49] O. Hinrichsen, F. Rosowski, M. Muhler, G. Ertl, Stud. Surf. Sci. Catal. 109 (1997) 389.
[50] O. Hinrichsen, A. Hornung, M. Muhler, Chem. Eng. Technol. 22 (1999) 1039.
[51] M. Crocoll, S. Kureti, W. Weisweiler, J. Catal. 229 (2005) 480.
[52] C.T. Campbell, G. Ertl, H. Kuipers, J. Segner, Surf. Sci. 107 (1981) 220.
[53] A.B. Mhadeshwar, H. Wang, D.G. Vlachos, J. Phys. Chem. B 107 (2003) 12721.